Bull. Mater. Sci., Vol. 33, No. 5, October 2010, pp. 611–618. © Indian Academy of Sciences.

Solution combustion synthesis of (La, K) FeO_3 orthoferrite ceramics: structural and magnetic property studies

MANJUNATH B BELLAKKI and V MANIVANNAN*
Department of Mechanical Engineering, Colorado State University, Fort Collins, Colorado, USA

MS received 13 March 2009

Abstract. **Polycrystalline $La_{1-x}K_xFeO_3$ ceramic oxides were synthesized by a solution combustion process using glycine as a fuel. The synthesized ceramic powders were characterized for structural features applying characterization techniques such as powder X-ray diffraction (XRD), scanning electron microscopy (SEM), Fourier transform infrared spectroscopy (FTIR), and magnetic and optical property studies applying characterization techniques such as SQUID magnetometer and diffuse reflectance (DR). The changes in magnetic properties are correlated to changes in structural features resulting from Rietveld structural refinement.**

Keywords. **Perovskite oxides; combustion synthesis; X-ray diffraction; antiferromagnet.**

1. Introduction

The rare-earth based ceramics have found profound applications in various technologies such as sensors (Xiaochuan *et al* 2006; Xing *et al* 2008), oxygen permeation membranes (Shaula *et al* 2005; Bayraktar *et al* 2007), electrodes in solid oxide fuel cells (Huang *et al* 2007; Bidrawn *et al* 2008) and environmental monitoring devices (Traversa *et al* 2000). These technological applications are due to unique structural features of perovskites which are largely influenced by processing conditions. A variety of synthesis techniques such as solid state (Smith and Norby 2006), sol–gel (Dai *et al* 2006), co-precipitation (Pecchi *et al* 2008), hydrothermal (Zheng *et al* 2000), polyol method (Maike *et al* 2007), etc have been employed to prepare these materials.

Despite success of the methods, there are several disadvantages associated with the synthesis such as long reaction times due to slow kinetics/diffusion, formation of secondary and/or impurity phases etc which we desire to overcome. A convenient method of synthesis, where oxide ceramics are synthesized by a simpler procedure (i.e. shorter time, less complex) without compromising the quality of the ceramic powder, is desired.

Among many perovskite ceramics, $LaFeO_3$ is of current interest as it has found applications in technologies such as solid oxide fuel cells (SOFCs) and photo catalysts. The application is due to favourable properties of the material, such as being a mixed (electronic and ionic) conductor (Huang *et al* 1998) due to creation of Fe^{3+}/Fe^{4+} mixed valence ions, beneficial band structure etc. For example, in anode-supported SOFCs, doped $LaFeO_3$ used as a cathode material showed improved conductivity, resulting in enhanced performance (Huang *et al* 1998; Simner *et al* 2003).

$LaFeO_3$ has been doped with bivalent metal ions like Sr^{2+}, Ca^{2+}, and Ba^{2+} (Bidrawn *et al* 2008). We envisaged that mixed valency can be induced by monovalent substitutions like K^+, which could lead to possible mixed conductivity in the system. Also, to facilitate synthesis of high quality ceramic powders in a cost-effective procedure, we intend to apply a solution-based combustion process using glycine as a fuel. Such an approach, i.e. $LaFeO_3$ doped with K^+, synthesized by a simple combustion method, has not been reported so far.

2. Experimental

$La_{1-x}K_xFeO_3$ ($0 \le x \le 0{\cdot}3$) perovskite ceramics were synthesized by the solution combustion method using glycine as a fuel. The detailed procedure for calculating the metal nitrates to fuel ratio has been described elsewhere (Patil *et al* 1997). Stoichiometric amounts of $La(NO_3)_3{\cdot}5H_2O$, KNO_3 and $Fe(NO_3)_3{\cdot}9H_2O$ were dissolved in a minimum amount of water in a pyrex dish. A calculated amount of the fuel glycine was added. The resulting aqueous solution was introduced into a muffle furnace maintained at 400°C. The mixture was boiled, followed by frothing, and ignited with evolution of a large amount of gases. The flame persisted for about a min leaving behind a residual black-coloured fine powder. The chemical reaction occurring in the combustion process can be written as:

$$(1-x)La(NO_3)_3(aq) + xK(NO_3)\,(aq) + Fe(NO_3)_3\,(aq) + C_2H_5NO_2\,(aq) \rightarrow La_{1-x}K_xFeO_3\,(s) + CO_2\,(g) + H_2O\,(g) + N_2(g). \quad (1)$$

*Author for correspondence (mani@engr.colostate.edu)

The phase purity and crystal structure were examined by a Bruker X-ray diffractometer using CuK_α radiation with a nickel filter. For Rietveld refinement, data were collected at a scan rate of 0·5°/min with a 0·02° step size for 2θ from 10–100°. The data were refined using the Foolproof Suite (2000 version). The morphology of the powder was examined using a JEOL JSM-840A scanning electron microscope fitted with an energy dispersive X-ray analyser (EDX). Infrared spectra of samples were recorded on a Thermo Nicolet FT–IR Spectrometer for a spectrum ranging from 400–4000 cm^{-1}. The magnetization measurements were performed using a SQUID magnetometer in the temperature range 2·5–300 K with a static applied field of 1000 Oe. Diffuse reflectance spectra were recorded in the wavelength range 250–2500 nm using a Varian Associated Cary 500 double beam spectrophotometer. Compressed polytetrafluoroethylene (PTFE) was used for standard calibration (100% reflectance).

2.1 *Determination of Fe^{3+}/Fe^{4+} concentration*

The ratio of the Fe^{3+}/Fe^{4+} concentration was determined by iodometric titration for all the samples (Singh *et al* 1998). Typically, about 50 mg of the compound was dissolved in 10 ml of 1 : 1 HCl containing about 1 g of solid KI. Liberated iodine was titrated against a standard potassium thiosulphate (0·05 N) solution using starch as an indicator.

3. Results and discussion

K substitution into $LaFeO_3$ was attempted at 10, 20, 30, and 40 at.%; single phase formation was limited to 30 at.% and accordingly, the current study was limited to 30 at.% materials. Impurities were noticed in the XRD pattern when K concentration exceeded 30%. Figure 1 shows the XRD pattern of $La_{1-x}K_xFeO_3$ ($0 \le x \le 0{\cdot}3$) single phase materials in comparison with the reported pattern in the literature (JCPDF No. 01-070-7777). $LaFeO_3$ crystallizes in orthorhombic symmetry having lattice parameters a = 5·554 Å, b = 5·562 Å, and c = 7·852 Å, with space group *Pbnm* (No. 62). The refined lattice parameters for the undoped and doped materials are summarized in table 1. In figure 2, observed, calculated and difference XRD patterns of the typical refined XRD patterns of (a) $LaFeO_3$ and (b) $La_{0.8}K_{0.2}O_3$, are given. There is a good agreement between the observed and calculated patterns. The refined structural parameters, selected bond lengths and bond angle are summarized for all the samples in table 1.

Figure 3 shows the effect of introducing potassium into the orthorhombic lattice resulting in slight decrease in a, b and c lattice parameters (figure 3). The cell volume decreased from 242·554–241·741 ($Å^3$) as the K content increased from 0·1 to 0·3 (inset, figure 3). The variations in lattice parameter are consistent with lattice parameter changes in $LaMnO_3$ as a result of K doping into the system (Guoyan *et al* 2007).

To understand the microstructural features of $La_{1-x}Na_xFeO_3$ ($0 \le x \le 0{\cdot}3$) samples, SEM was performed (figure 4). SEM showed that the microstructure consisted of submicron size particles. The particles of $LaFeO_3$ (figure 4a) and $(La_{0.8}K_{0.2})FeO_3$ (figure 4b) are agglomerated and already connected together to form a porous or open structure. The 'necking' observed for the ceramic powders could be favourable in preserving the electrical conductivity of the materials. EDX in combination with SEM showed that the synthesized ceramics have a homogeneous composition.

FTIR spectra of the (La, K) FeO_3 ceramics are given in figure 5. The bands in the wave number regions 650–500 and 430–400 cm^{-1} are due to the asymmetric stretching vibrations of Fe–O–Fe bonds and deformation of FeO_6 octahedra, respectively in the $LaFeO_3$ oxide (Davydov 1990). The higher frequency band at 600 cm^{-1} was assigned to the Fe–O stretching vibration mode, which involves internal motion of a change in Fe–O bond length, and the lower band around 450 cm^{-1} corresponds to the bending mode, which is indicative of any changes in the Fe–O–Fe bond angle. Figure 5 also shows that on

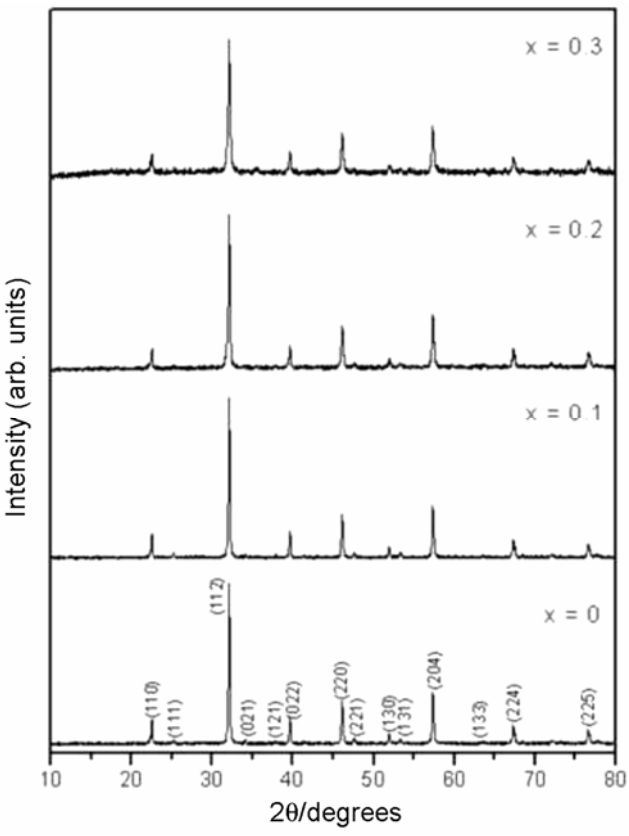

Figure 1. Powder XRD patterns of $La_{1-x}K_xFeO_3$ ($0{\cdot}0 \le x \le 0{\cdot}3$) phases.

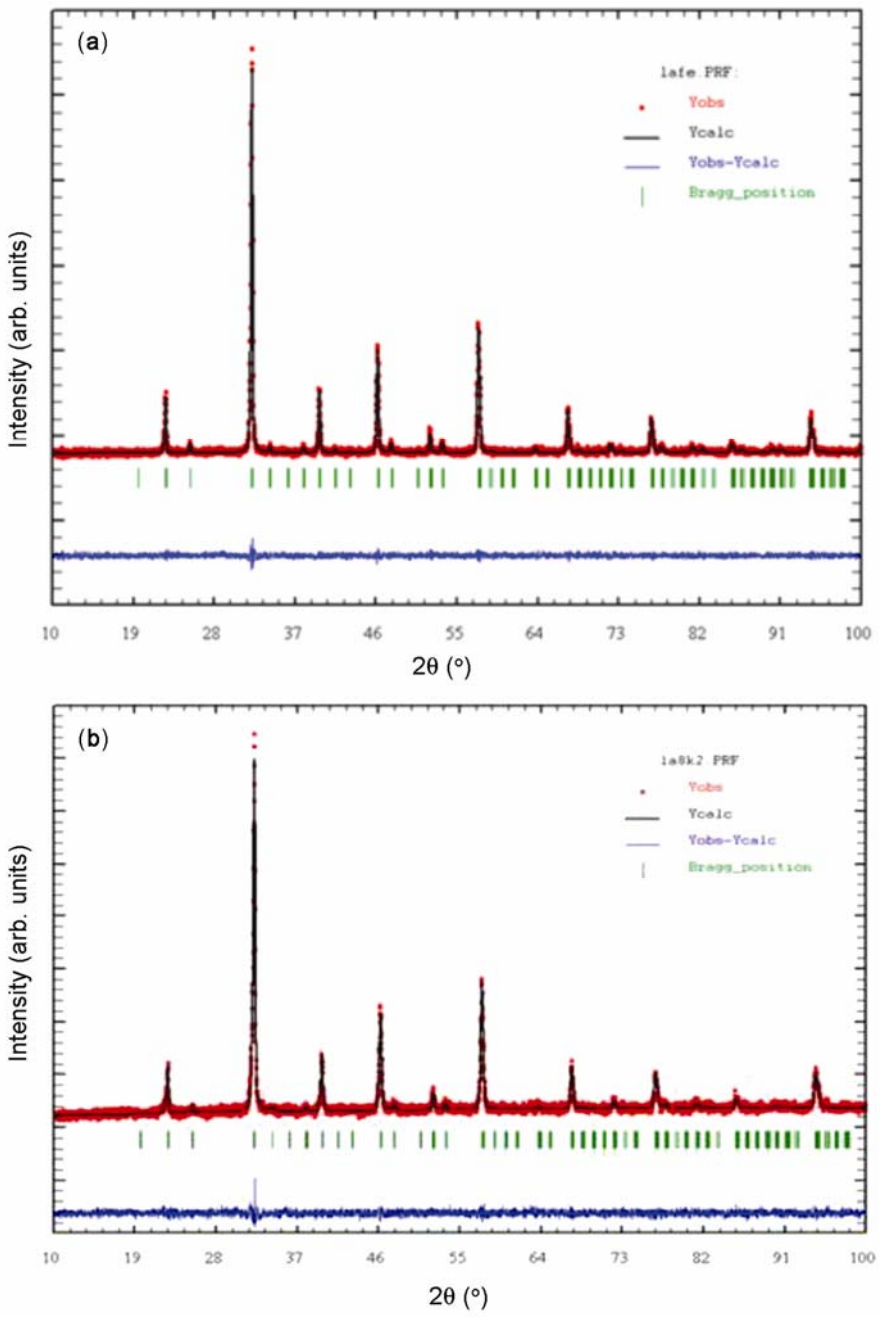

Figure 2. Typical, observed, calculated and difference Rietveld refined XRD pattern of (**a**) $LaFeO_3$, and (**b**) $La_{0·80}K_{0·20}FeO_3$.

increasing K content to $x = 0·3$, the band at 560 cm^{-1} shifts to higher wave numbers and increases in intensity compared to the undoped orthoferrite ceramics. In the doped sample the bands around 1400 cm^{-1} are attributed to surface-adsorbed carbonate group species (Yoshihiko *et al* 1995).

Magnetization results for (La, K) FeO_3 ceramic oxide are shown in figure 6. Figure 6a shows the temperature dependence of the molar magnetic susceptibility (χ_M) at a magnetic field of 1000 Oe. For the undoped $LaFeO_3$ material, χ_M is nearly zero, and with K doping, χ_M increases. Figure 6b shows the increased magnetization for all the samples at 25 K. The hysteresis loop for $x = 0·3$ material showed an increase in the magnetization value at a given field, which is in consistency with the data given in figure 6a.

The structural features of $LaFeO_3$ position them for potential applications. For example, the sensor applications of $LaFeO_3$ are largely dependent on the effects of surface and quantum confinement (Li *et al* 2000). The

Table 1. Rietveld refined structural parameters for $La_{1-x}K_xFeO_3$ ($0 \le x \le 0{\cdot}3$) phases.

Compounds	$LaFeO_3$	$La_{0{\cdot}90}K_{0{\cdot}10}FeO_3$	$La_{0{\cdot}80}K_{0{\cdot}20}FeO_3$	$La_{0{\cdot}70}K_{0{\cdot}30}FeO_3$
Crystal system		Orthorhombic		
Space group		*Pbnm* (62)		
Lattice parameters				
a (Å)	5·554(2)	5·553(3)	5·551(3)	5·550(6)
b (Å)	5·562(3)	5·558(3)	5·557(6)	5·554(5)
c (Å)	7·852(4)	7·850(7)	7·845(5)	7·841(5)
Cell volume (Å^3)	242·55(4)	242·26(5)	242·02(1)	241·74(4)
Bond lengths (Å)				
Fe_1–O_1	2·008(5)	2·007(6)	2·006(3)	2·005(8)
Fe_1–O_2'	1·988(4)	1·977(7)	1·971(6)	1·962(5)
Fe_1–O_2''	2·025(2)	2·035(2)	2·042(3)	2·041(5)
Bond angles (°)				
Fe–O_1–Fe	155·77(5)	155·86(3)	155·89(2)	155·85(3)
Fe–O_2–Fe	156·62(1)	156·49(4)	156·32(2)	157·43(5)

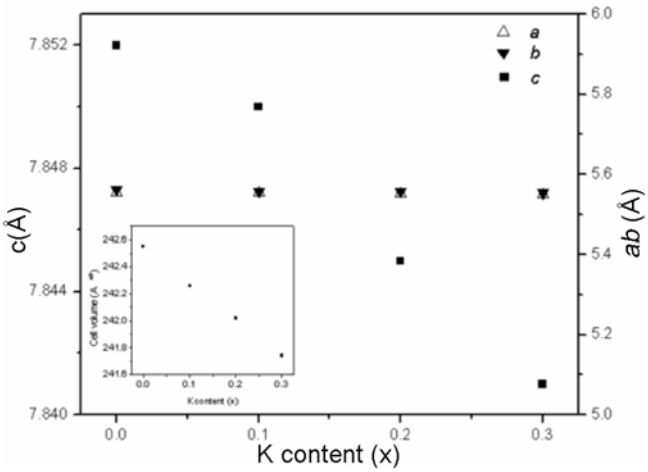

Figure 3. Plot of lattice parameters *a*, *b* and *c* vs K content (inset shows variation of cell volume vs K content).

photo catalytic activity of $LaFeO_3$ under visible irradiation occurs largely by photo-induced charge properties (Shudan *et al* 2007). The optical properties of $LaFeO_3$ influence its photo-induced charge properties; in this context it is important to know the bandgap of $LaFeO_3$ and its variation as a result of K doping.

In order to determine the energy bandgap of (La, K) FeO_3 ceramic oxides in conjugation with structural features, we have performed DR measurements. Figure 7(a) shows the diffuse reflectance spectra of $La_{1-x}K_xFeO_3$ ($0 \le x \le 0{\cdot}3$) samples in the UV–vis–NIR range. The diffuse reflectance data was used to calculate the absorption coefficient from the Kubelka–Munk (KM) function (Kubelka and Munk 1931; Kortum 1969) defined as:

$$F(R_\infty) = \alpha/S = (1 - R_\infty)^2/2R. \quad (3)$$

where $R_\infty = R_{sample}/R_{PTFE}$.

Here α is the absorption coefficient, S the scattering coefficient, and $F(R_\infty)$ the KM function. The energy dependence of the material in the UV–vis–NIR range was further explored. The energy dependence of semiconductors near the absorption edge is expressed as:

$$\alpha E = K(E - E_g)^\eta. \quad (4)$$

Here E is the incident photon energy ($h\nu$), E_g the optical absorption edge energy, K is a constant, and the exponent η is dependent on the type of optical transition as a result of photon absorption (Barton *et al* 1999). The exponent η is assigned a value of 1/2, 3/2, 2, and 3 for direct allowed, direct forbidden, indirect allowed, and indirect forbidden transition, respectively (Tauc *et al* 1966).

For the diffused reflectance spectra, the KM function can be used instead of α for estimation of the optical absorption edge energy (Barton *et al* 1999). It was observed that, for a plot of $F(R_\infty)$, E vs E (figure 7(b)) was linear near the edge for direct allowed transition ($\eta = 1/2$). The intercept of the line on the abscissa ($F(R_\infty)$ $E = 0$) gave the value of optical absorption edge energy. The values were determined to be $2{\cdot}4 \pm 0{\cdot}2$, $2{\cdot}1 \pm 0{\cdot}2$, $1{\cdot}85 \pm 0{\cdot}2$, and $1{\cdot}6 \pm 0{\cdot}2$ eV for $x = 0$, 0·1, 0·2 and 0·3, respectively. The diffuse reflectance spectra for direct bandgap orthorhombic (β) (Sahu and Kleinman 2004) prepared by heating Ta metal in air are also recorded for comparison. The value of optical absorption edge energy for the indirect allowed transition for Ta_2O_5 was found to be $4{\cdot}0 \pm 0{\cdot}2$ eV, which is consistent with those seen for the β-Ta_2O_5 reported (Knausenberger and Tauber 1973).

When K is doped into $LaFeO_3$ ceramics, there are significant changes in the properties of the materials associated with the building block of perovskite structure – FeO_6 octahedra (figure 8a). FeO_6 octahedra get distorted due to K doping, resulting in changes in both Fe–O–Fe

bond lengths and bond angles. The Fe–O–Fe bond angle is a measure of the tilting of the octahedron and the Fe–O–Fe bond length is related to the buckling of the octahedron. Rietveld structural refinement showed with increased K substitution, the in-plane bond length (Fe_1–O_2') decreased progressively from 1·988 Å (for $x = 0$) to 1·962 Å at 30% K doping of $LaFeO_3$. Similarly the apical bond length (Fe_1–O_1) decreased from 2·008 Å–2·005 Å in a similar fashion. Also, the in-plane Fe–O_2–Fe bond angle decreased from 156·62° to 156·32° for K doping up to 20%. Similarly, the cooperative tilting of FeO_6 octahedra resulted in apical bond angles; overall, the Fe–O_1–Fe angle changes from 155·77–155·85°.

Chemical titration on (La K) FeO_3 showed that with progressive K substitution, Fe^{4+} increased disproportionately relative to Fe^{3+}, creating a mixed valency in the sys-

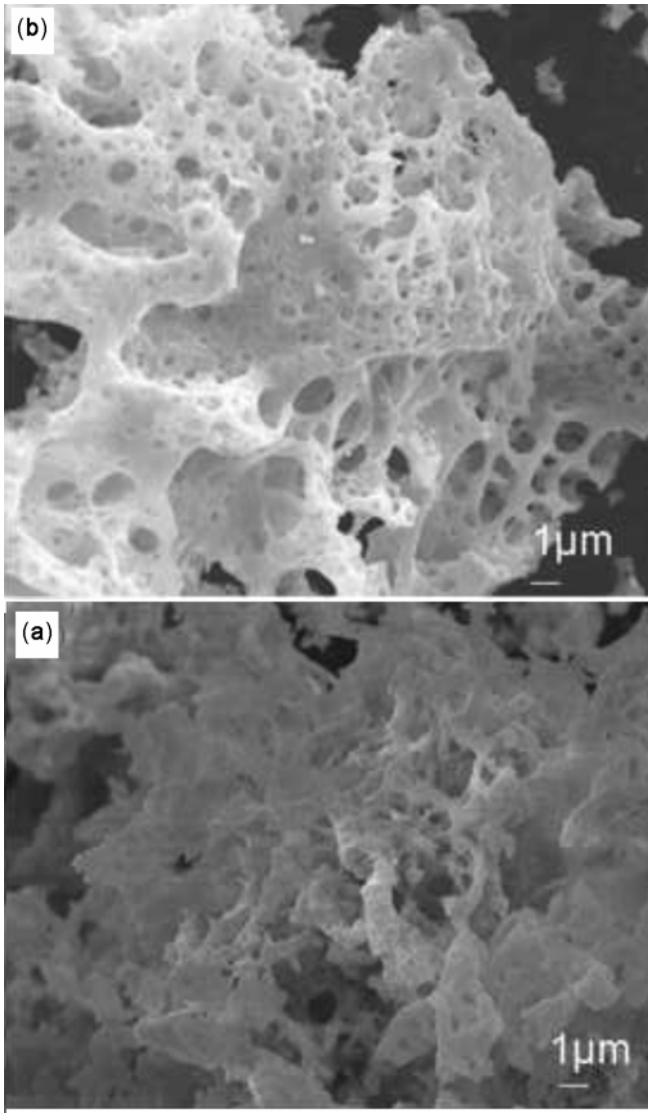

Figure 4. Scanning electron micrographs of (**a**) $LaFeO_3$, and (**b**) $La_{0·80}K_{0·20}FeO_3$.

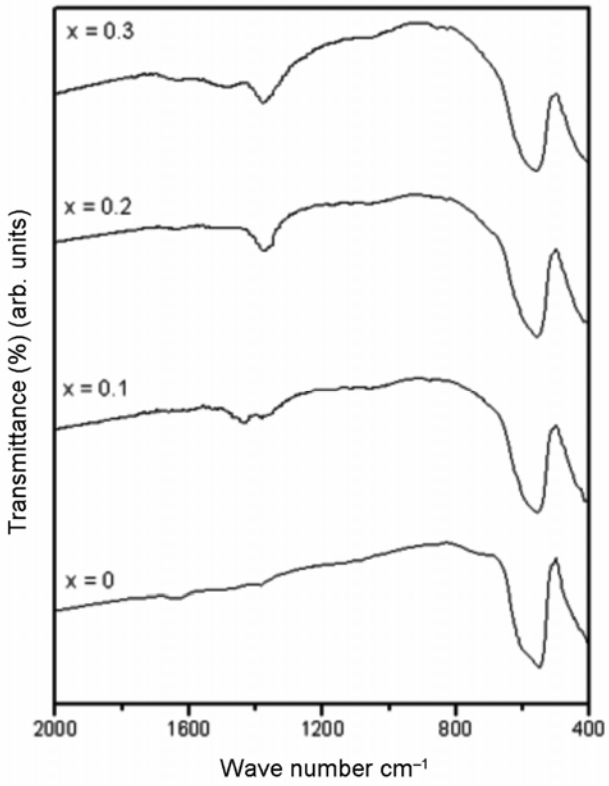

Figure 5. FTIR spectra of $La_{1-x}K_xFeO_3$ ($0·0 \le x \le 0·3$) phases.

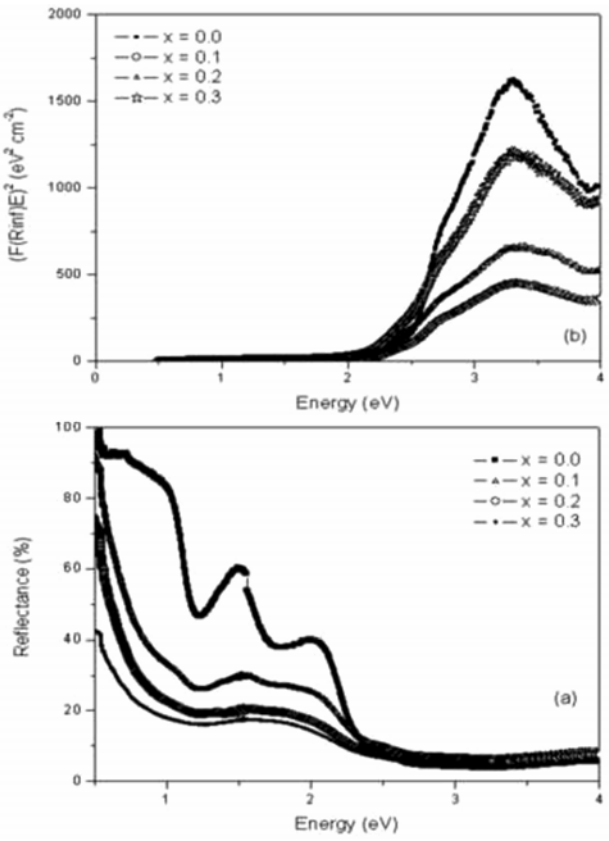

Figure 6. (**a**) Molar magnetic susceptibility (χ_m) vs temperature as a function of applied field, and (**b**) hysteresis loop measured at 25 K for $La_{1-x}K_xFeO_3$ ($0·0 \le x \le 0·3$) phases.

Table 2. Values of oxygen stoichiometry, Fe^{4+} content, magnetic susceptibility, and magnetic moment of $La_{1-x}K_xFeO_3$ phases.

$La_{1-x}K_xFeO_3$	Fe^{4+} content (%)	χ_M (at 2·5 K)	μ_B (at 2·5 K)$_{BM}$
$x = 0$	3·8	0·035	0·031
$x = 0·1$	19·3	0·288	0·258
$x = 0·2$	29·4	0·342	0·306
$x = 0·3$	35·1	0·653	0·649

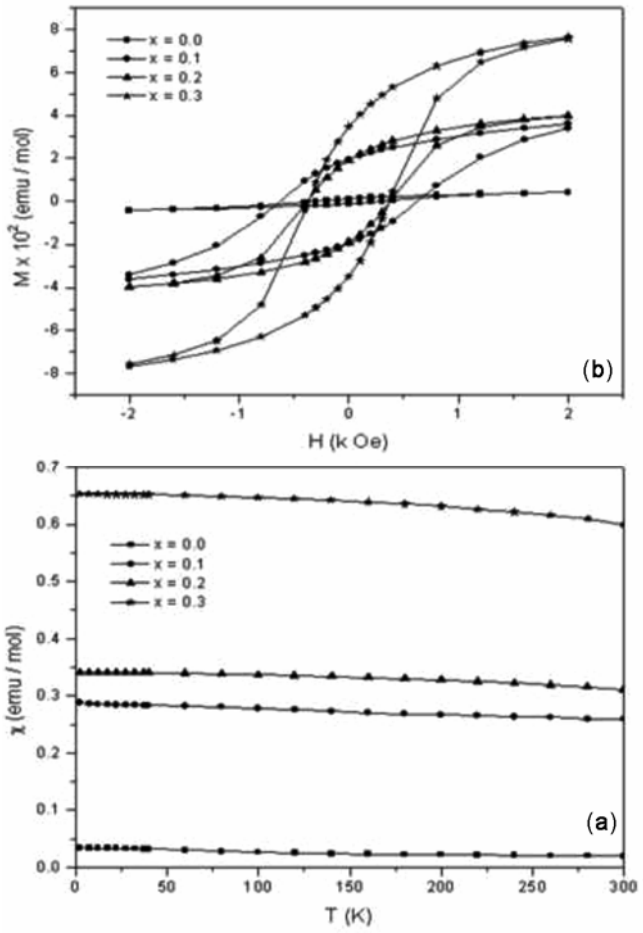

Figure 7. (**a**) UV–Vis absorption and (**b**) diffuse reflectance spectra of $La_{1-x}K_xFeO_3$ ($0·0 \le x \le 0·3$) phases.

tem. The parent compound contained a small percentage of Fe^{4+} (3·8%); it increased to 35·1% when 30% K was substituted. The effect of K doping (to compensate for cation deficiency) into $LaFeO_3$ are three-fold: (a) creation of a mixed valency state, (b) occurrence of O_2 vacancies, and (c) a state intermediate to (a) and (b) (Yamamura *et al* 1981). Rietveld refinement showed that the oxygen stoichiometry decreased from $O_{3·08}$ for the parent orthoferrites to $O_{2·90}$, $O_{2·81}$, $O_{2·71}$ for 10%, 20% and 30% K doping, respectively. Rietveld refinement, in conjunction with iodometry titration, indicates that condition (c) is a possibility. Such a situation is similar to $SrFeO_{3-\delta}$, the sample of which is synthesized in air, has both a O_2 vacancy and a mixed valency of Fe (Yamamura *et al* 1981). The final formula has been given for each composition in table 1.

The observed changes in the magnetic properties, i.e. magnetic moment, of pure $LaFeO_3$, is nearly zero; as a result it increases with K doping along with an increase in magnetization. This could be understood from the canted-antiferromagnetic (AFM) behaviour of these materials. It is known that $LaFeO_3$ exhibits G-type AFM behaviour (see figure 8b) (Shein *et al* 2005). The canting of the Fe spins at small angles is due to exchange coupling resulting in a small net magnetic moment (table 2), with increase in Fe^{4+} content due to K doping and net magnetic moment increase. In addition, the presence of oxygen vacancies disturb antiparallel spin ordering in the Fe^{3+}–O–Fe^{3+} linkage (called a super exchange interaction).

4. Applications

Shudan *et al* (2007) showed that nanostructural $LaFeO_3$ ceramics had superior photo catalytic activity relative to standard TiO_2, the efficiency of which is low due to a wide bandgap (3·2 eV) (Hoffmann *et al* 1995). The surface photo voltage spectroscopy signal of $LaFeO_3$ nanoparticles is attributed to the favourable band–structure involving electronic transitions from the valence band to conduction band [$Fe_{3d} \rightarrow O_{2p}$] (Li *et al* 2000). The lower bandgap of $LaFeO_3$ ceramics compared to TiO_2 and the nanoparticulate nature of these ceramics could position them as promising photo catalytic materials.

Perovskite manganite materials like (La, Sr) MnO_3 are used as cathodes in ZrO_2 based SOFCs mainly due to attractive electronic conductivity properties. In the absence of ionic conduction or creation of oxygen vacancies, a thick electrode is needed to achieve the desired catalytic activity (Huang *et al* 1998). The (La, Sr)CoO_3 on the other hand has shown to possess oxide-ion conduction making the cobalt perovskite an useful electrode material due to the mixed (electronic and ionic) conduction (Feng *et al* 1996). K-doped $LaFeO_3$, with mixed valency Fe^{3+}/Fe^{4+} as well as oxygen vacancy, has the potential to be a cathode material for SOFC applications.

5. Conclusions

Ceramic ferrite, $LaFeO_3$, was synthesized by a simple solution combustion process. Potassium doping up to

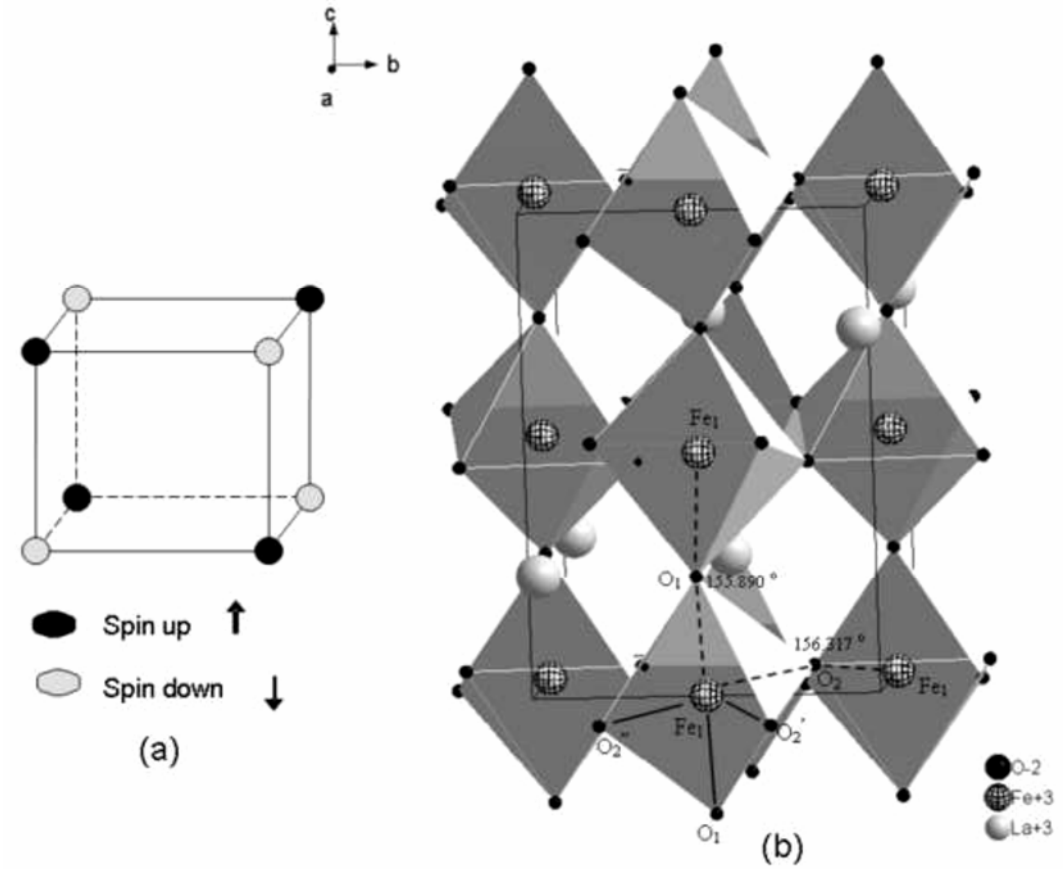

Figure 8. Typical (**a**) schematic drawing of tilted FeO_6 octahedra in $La_{0.8}K_{0.2}FeO_3$, and (**b**) antiferromagnetic (*G*) types of collinear spin ordering (in the iron sublattice).

30 at.% into $LaFeO_3$ is possible without forming any impurities. Detailed structural refinement was carried out for the orthoferrite ceramic materials and the corresponding magnetic and optical properties were determined. The observed changes in the magnetic properties are correlated to the presence of a Fe^{3+}/Fe^{4+} mixed valency. K doping of $LaFeO_3$ has positioned the ceramic oxide material for potential applications such as cathode material for SOFCs and as an electrode for photo catalysts.

Acknowledgement

The authors would like to acknowledge Prof. Allan Kirkpatrick, Department of Mechanical Engineering, Colorado State University, USA, for his continued help, encouragement and support.

References

Barton D G, Shtein M, Wilson R D, Soled S L and Iglesia E 1999 *J. Phys. Chem.* **B103** 630

Bayraktar D, Clemens F, Diethelm S, Graule T, Van H J and Holtappels P 2007 *J. Euro. Ceram. Soc.* **27** 2455

Bidrawn F, Lee S, Vohs J M and Gorte R J 2008 *J. Electro. Chem. Soc.* **155** 660

Dai X P, Li R J, Yu C C and Hao Z P 2006 *J. Phys. Chem.* **B110** 22525

Davydov A 1990 *Infrared spectroscopy of adsorbed species on surface of transition metal oxides* (England: Wiley) Ch. 1

Feng M, Goodenough J B, Huang K and Milliken C 1996 *J. Power. Sources* **30** 110

Guoyan H, Zhijun G, Shuang L, Ye W and Yuping W 2007 *J. Alloys Compd* **433** 41

Hoffmann M R, Martin S T, Choi W and Bahnemann D W 1995 *Chem. Rev.* **95** 69

Huang K, Lee H Y and Goodenough J B 1998 *J. Electrochem. Soc.* **45** 3220

Huang M H, Madhava Rao M V and Tsai D S 2007 *Mater. Chem. Phys.* **101** 297

Knausenberger W H and Tauber R N 1973 *J. Electrochem. Soc.* **120** 927

Kortum G 1969 *Reflectance spectroscopy principles, methods, applications* (New York: Springer-Verlag)

Kubelka P and Munk F 1931 *J. Tech. Phys.* **12** 593

Li K, Wang D, Wu F, Xie T and Li T 2000 *Mater. Chem. Phys.* **64** 269

Maike S, Leifert A and Simon U 2007 *Adv. Funct. Mater.* **17** 2189

Patil K C, Aruna S T and Ekambaram S 1997 *Curr. Opin. Solid St. M.* **2** 158

Pecchi G, Reyes P, Zamora R, Campos C, Cadus L E and Barbero B P 2008 *Catal. Today* **133** 420

Sahu B R and Kleinman L 2004 *Phys. Rev.* **B69** 165202

Shaula A L, Kharton V V, Vyshatko N P, Tsipis E V, Patrakeev M V, Marques F M B and Frade J 2005 *J. Euro. Ceram. Soc.* **25** 489

Shein I R, Shein K I, Kozhevnikov V L and Ivanovskii A L 2005 *Phys. Solid State* **47** 2082

Shudan Li, Liqiang J, Wei F, Libin Y, Baifu X and Honggang F 2007 *Mater. Res. Bull.* **42** 203

Simner S P, Shelton J P, Anderson M D and Stevenson J W 2003 *Solid State Ionics* **161** 11

Singh R N, Shivakumara C, Vasanthacharya N Y, Subramanian S, Hegde M S, Rajagopal S and Sequeira A 1998 *J. Solid State Chem.* **137** 19

Smith J B and Norby T 2006 *Solid State Ionics* **177** 639

Tauc J, Grigorov R and Vancu A 1966 *Phys. Status Solidi* **15** 627

Traversa E, Sadaoka Y, Carotta M C and Martinelli G 2000 *Sensors Actuators* **B65** 181

Xiaochuan L, Huiming J, Yanfei G and Mingxia X 2006 *Mater. Sci. Eng.* **B133** 98

Xing L, Bin C, Jifan H, Hongwei Q and Minhua J 2008 *Sensors Actuators* **B129** 53

Yamamura H, Haneda H and Shirasaki S I 1981 *J. Solid State Chem.* **36** 1

Yoshihiko S, Kazuaki W, Yoshiro S and Masatomi S 1995 *J. Alloys Compd* **224** 194

Zheng W, Liu R, Peng D and Meng G 2000 *Mater. Lett.* **43** 19